iScience

Article

OSBPL2 deficiency alleviates diet-induced MASLD by reducing ACSL4-mediated ferroptosis

Graphical abstract

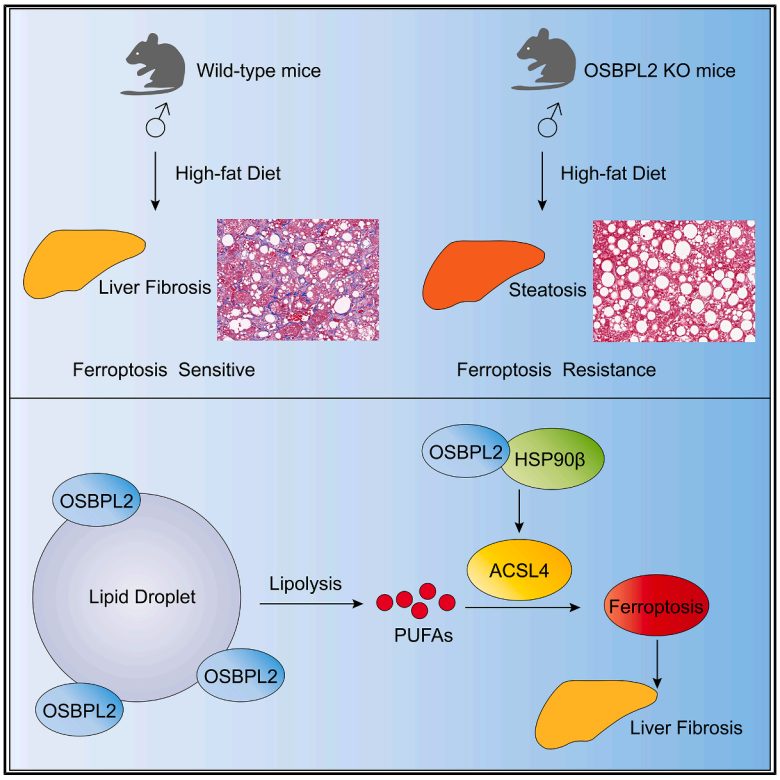

Highlights

- OSBPL2 modulates hepatic fatty acid distribution through the regulation of lipolysis
- OSBPL2 binds to HSP90β to regulate ACSL4 expression
- Depletion of OSBPL2 confers ferroptosis resistance through the ACSL4/PUFA pathway
- OSBPL2 knockout mitigates diet-induced liver fibrosis by suppressing ferroptosis

Authors

Tianming Wang, Fanghong Sheng, Chao Lian, ..., Xin Cao, Xuemei Chen, Jianquan Chen

Correspondence

caoxin@njmu.edu.cn (X.C.), 13347808579@189.cn (X.C.), jqchen@njmu.edu.cn (J.C.)

In brief

Biochemistry; Molecular biology; Cell biology

Wang et al., 2026, iScience *29*, 115478
April 17, 2026
https://doi.org/10.1016/j.isci.2026.115478

CellPress

iScience

CellPress
OPEN ACCESS

Article

OSBPL2 deficiency alleviates diet-induced MASLD by reducing ACSL4-mediated ferroptosis

Tianming Wang,[1,2] Fanghong Sheng,[3] Chao Lian,[1,2] Zhengyuan Lv,[3] Jun Yao,[3] Xin Cao,[3,*] Xuemei Chen,[2,4,*] and Jianquan Chen[1,2,5,*]

[1]Central Laboratory, The Affiliated Jiangning Hospital with Nanjing Medical University, Nanjing, Jiangsu, China
[2]Translational Medicine Research Center, The Affiliated Jiangning Hospital with Nanjing Medical University, Nanjing, Jiangsu, China
[3]Department of Medical Genetics, School of Basic Medical Science, Nanjing Medical University, Nanjing, China
[4]Department of Neurology, Affiliated Jiangning Hospital with Nanjing Medical University, Nanjing, Jiangsu, China
[5]Lead contact
*Correspondence: caoxin@njmu.edu.cn (X.C.), 13347808579@189.cn (X.C.), jqchen@njmu.edu.cn (J.C.)
https://doi.org/10.1016/j.isci.2026.115478

SUMMARY

Oxysterol-binding protein-like 2 (OSBPL2) is a lipid transfer protein that modulates intracellular lipid homeostasis; however, its regulatory role in coordinating iron and fatty acid homeostasis remains largely elusive. A recent study has reported a strong positive correlation between iron overload and the progression of metabolic dysfunction-associated steatotic liver disease (MASLD). Herein, we found that OSBPL2 binds to HSP90β, and OSBPL2 deficiency inhibits ACSL4 expression while altering hepatic fatty acid distribution by impairing lipolysis. Depletion of OSBPL2 conferred resistance to ferroptosis via the ACSL4-mediated ferroptosis pathway and further attenuated diet-induced liver fibrosis in mice. Our findings provide important insights into the function of OSBPL2 in ferroptosis and suggest that OSBPL2 may serve as a potential therapeutic target for MASLD.

INTRODUCTION

Non-alcoholic fatty liver disease (NAFLD), now renamed metabolic dysfunction-associated steatotic liver disease (MASLD), stands as one of the most severe chronic diseases.[1] It encompasses simple hepatic steatosis, non-alcoholic steatohepatitis (NASH), NASH with fibrosis, and cirrhosis that progresses to end-stage liver disease.[2] Simple hepatic steatosis is often considered benign, whereas fibrosis is regarded as more clinically relevant due to its detrimental effects on liver function. Currently, clinical management of MASLD primarily relies on lifestyle interventions such as dietary adjustments and increased physical activity, which often have limited efficacy. In recent years, however, there has been a growing focus on research aimed at elucidating the molecular mechanisms underlying MASLD pathogenesis and exploring more effective preventive and therapeutic strategies.

MASLD is characterized by intrahepatic lipid accumulation. Excess free fatty acids (FFAs) are esterified into triacylglycerols (TAGs) and then stored within lipid droplets (LDs).[3] LDs, which enclose a core filled with neutral lipids surrounded by a phospholipid monolayer, are intracellular dynamic organelles that regulate intracellular lipid balance in accordance with energy requirements. Triglyceride lipolysis within LDs can be catalyzed step-by-step into FFAs by multiple lipases.[4] In white adipose tissue, a single large LD occupies most of the cellular space, whereas in hepatocytes, there are numerous relatively small LDs. Oxysterol-binding protein-like 2 (OSBPL2) is a crucial lipid transporter protein responsible for regulating dynamic shifts in cell membranes; it accomplishes this by transporting cholesterol and mediating cholesterol exchange within cell membranes.[5] Previous studies on various animal models have revealed that OSBPL2 deficiency leads to cholesterol accumulation and phenotypes resembling obesity.[6–8] Additionally, we have observed LD accumulation in OSBPL2-knockout (KO) cells.[9] Therefore, we speculate that OSBPL2 is involved in regulating lipid balance within hepatocytes and thereby influences the occurrence and progression of MASLD.

Ferroptosis, a research topic that has attracted considerable attention in recent years, is not limited to tumors but also occurs in various physiological and pathological processes triggered by abnormal iron metabolism. Ferroptosis primarily induces oxidative damage by integrating peroxidized lipids into the cellular membrane structure.[10] Common triggers of ferroptosis include impairment of the antioxidant defense function of System Xc−, catalysis of polyunsaturated fatty acids (PUFAs) to form peroxidized lipids by ACSL4, and disruption of the ubiquinone cycle. A recent report demonstrated iron deposition in liver tissues of patients with MASLD, highlighting the critical role of long-chain fatty acid–CoA ligase 4 (ACSL4)/PUFA-mediated ferroptosis in liver fibrosis in mice.[11] Based on these findings, we hypothesize that OSBPL2 may affect ferroptosis by regulating fatty acid distribution within hepatocytes in MASLD.

In this study, wild-type (WT) mice and OSBPL2-KO mice were fed a high-fat diet (HFD) to establish a MASLD mouse model. Targeted metabolomics and proteomics were performed to

screen for differential fatty acids and differential proteins. The OSBPL2-KO HepG2 cell line and OSBPL2 knockdown Huh7 cell line were used to investigate the function of OSBPL2. Our results demonstrate that OSBPL2 deficiency alters fatty acid distribution, causes LD accumulation, and suppresses hepatic ferroptosis via the ACSL4/PUFA pathway, thereby delaying the onset of liver fibrosis. This study provides novel perspectives for the early prevention of MASLD.

RESULTS

OSBPL2 deficiency causes fatty acids alteration and lipolysis inhibition in HepG2 cells

In our previous study, we established that OSBPL2 is crucial for the proper localization of lipase on LDs, and the lack of OSBPL2 delays lipolysis, resulting in the accumulation of LDs.[9] To reconfirm this finding, the OSBPL2-KO HepG2 cell line and its WT counterpart were selected (Figure 1A). As shown in Figure 1B, LDs in KO cells appeared larger compared to those in WT cells treated with either oleic acid (OA) or cholesterol. Consequently, we employ targeted metabolomics specifically focusing on medium and long-chain fatty acids to assess their abundance within hepatocytes. There were 6 repeats of KO cells and WT cells. Orthogonal Partial Least Squares Discriminant Analysis (OPLS-DA) showed distinct differences in metabolites between KO and WT group (Figure 1C). There were 13 differentially expressed metabolites (DEMs) out of 51 detectable fatty acids ($|\log_2 FC| > 1$ and $p < 0.05$), all of them were downregulated (Figure 1D). Among the Kyoto Encyclopedia of Genes and Genomes (KEGG) pathways, biosynthesis of unsaturated fatty acids, fatty acid biosynthesis, linoleic acid metabolism, ferroptosis, and GnRH signaling pathway showed the top 5 highest enrichment level (Figure 1E). These results suggested that plenty of fatty acids were reduced in KO cells, further indicating that OSBPL2 deficiency changed fatty acid distribution.

In general, excessive hepatic fatty acids are stored as triglycerides in LDs exhibiting a remarkable stability. When liver glycogen is depleted rapidly while the body still requires a large amount of energy, lipase becomes active. This leads to the gradual lipolysis of triglycerides, converting them into FFAs.[4] These FFAs then migrate to mitochondria or peroxisomes for β-oxidation, generating energy. We then induced LD formation with OA and monitored their lipogenesis and lipolysis progress by labeling LD with a fluorescence probe (BODIPY 493/503). Aligning with our earlier findings, after inducing LDs with OA for 24 h and subsequently culturing them in a basic medium devoid of fatty acids to promote lipolysis, we noticed a significant decrease in the number and size of LD in WT cells after 72 h but many large LDs remained accumulated in KO cells (Figures 1F and 1G). There was no substantial difference in LDs between the two groups within the first 8 h of OA treatment (Figure 1H). We also found that there were no significant differences in the expression of fatty acid synthase (FASN) and Stearoyl-CoA desaturase (SCD1) between WT and KO cells (Figure 1I). This result suggests that OSBPL2 deficiency does not affect *de novo* fatty acid synthesis.

Taking together, this finding underscores the role of OSBPL2 deficiency in affecting the fatty acids distribution and lipolysis process in HepG2 cells.

OSBPL2 deficiency changes hepatic fatty acids distribution and leads to hepatic LD accumulation in mice

To further clarify the correlation between OSBPL2 function and hepatic fatty acid distribution, we first investigated the expression of OSBPL2 in MASLD. A HFD-fed mouse model was established to simulate the phenotype of human MASLD. As shown in Figure 2A, mice in the HFD group exhibited significantly higher body weight compared to those in the CD group. The H&E staining results revealed enlarged adipocytes in the visceral adipose tissue of the HFD group, along with numerous LDs in their liver tissues (Figure 2B). To verify the expression level of OSBPL2 in the liver tissues of both groups, qPCR and immunohistochemistry (IHC) assays were performed. The qPCR results indicated a significant increase in the mRNA expression of OSBPL2 in the HFD group compared to the CD group (Figure 2C). Additionally, IHC results demonstrated more pronounced staining of OSBPL2 in the liver tissue of the HFD group (Figures 2D and 2E). These findings suggest that a HFD contributes to elevated expression of OSBPL2 in the liver.

Consequently, we employed targeted metabolomics specifically focusing on medium- and long-chain fatty acids to assess their abundance within the mouse liver. Five pairs of liver tissues were collected from KO and WT mice. OPLS-DA showed distinct differences in metabolites between the KO and WT group (Figure 2F). There were 11 DEMs among 51 detectable metabolites ($|\log_2 FC| > 1$ and $p < 0.05$), with 1 upregulated and 10 downregulated fatty acids (Figure 2G). The KEGG database showed 26 pathways enriched with metabolites of interest, which distinguished the KO and WT liver tissues. Among these pathways, biosynthesis of unsaturated fatty acids, fatty acid biosynthesis, linoleic acid metabolism, ferroptosis, and GnRH signaling pathway showed the top 5 highest enrichment levels (Figure 2H). These findings further supported our targeted metabolomics analysis of HepG2 cells that Osbpl2 deficiency altered fatty acid distribution.

Then the OSBPL2-KO mice and their littermate WT mice were randomly allocated to be fed a CD or a HFD. As shown in Figures 2I and S1A, HFD significantly increased the body weight of mice, but there was no significant difference in body weight between the KO group and the WT group either under HFD conditions or CD conditions. Subsequently, we fixed and stained the liver tissues of the mice. As shown in Figures 2J and S1D, H&E staining revealed the presence of lipid vacuoles in the livers of both WT and KO mice fed an HFD. The Oil Red O staining results indicated that HFD feeding caused an accumulation of LDs in mouse hepatocytes, suggesting the occurrence of hepatocyte steatosis (Figures 2K and S1E). According to the Oil Red O staining results, we observed more LDs in the liver tissues of the KO group than in those of the WT mice fed a CD, and a similar trend was also found in the mice fed an HFD. These results indicated that Osbpl2 deficiency caused hepatic LD accumulation in mice.

The above findings suggested that OSBPL2 was upregulated in HFD-induced liver tissue in mice, and that the lack of Osbpl2 altered hepatic fatty acid distribution and resulted in hepatic LD accumulation.

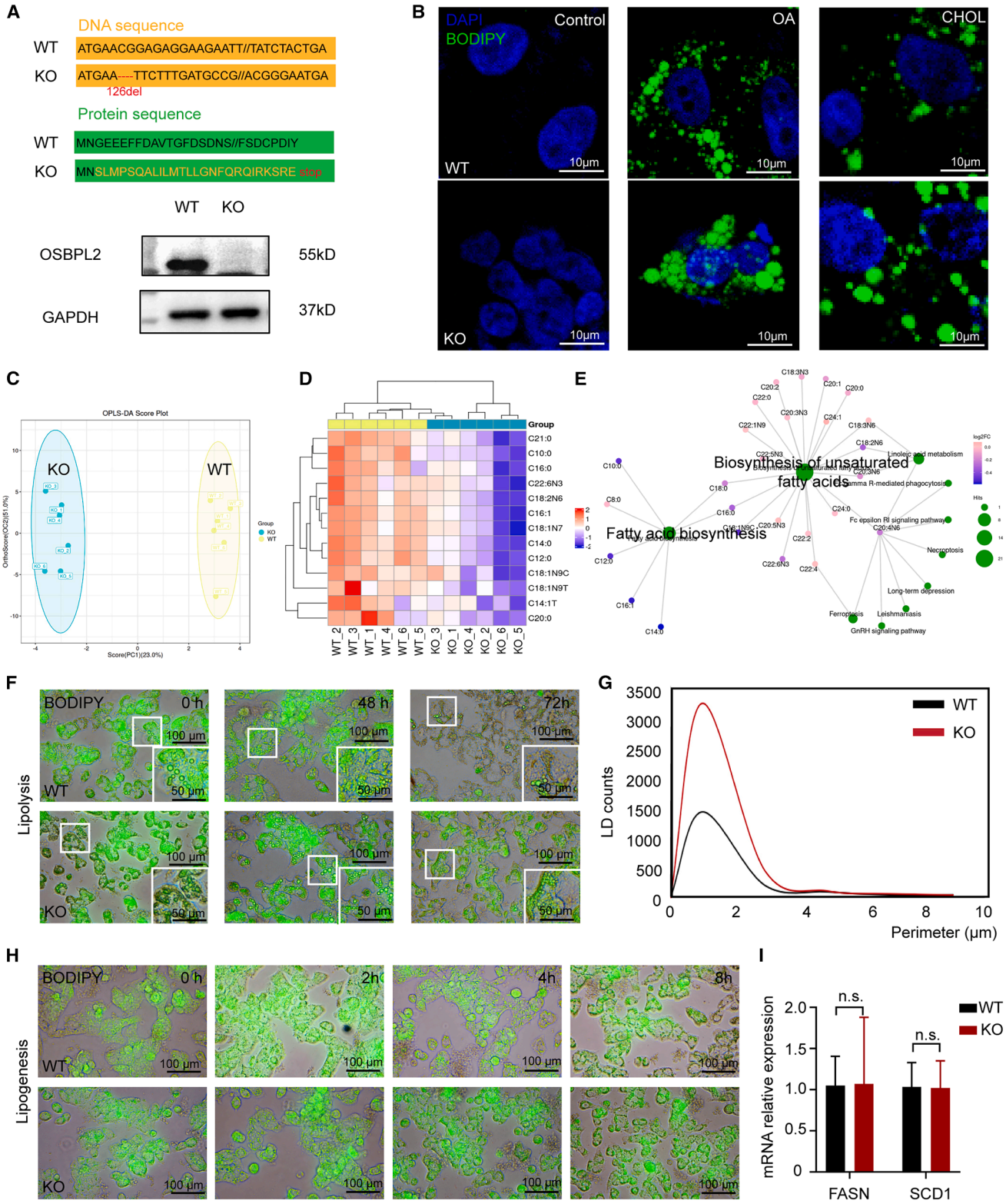

Figure 1. Fatty acids distribution and LD characteristics in OSBPL2-deficient HepG2 cell line

(A) Sequencing chromatogram of OSBPL2 allelic mutations in the KO cells compared with the WT cells. Lysates of the cells were immunoblotted for OSBPL2 and GAPDH. The data are normalized to the GAPDH control.

(legend continued on next page)

Proteomics reveals metabolic processes and signaling pathways in the KO cells

Consequently, we employed data-independent acquisition quantitative proteomics to detect and quantify proteins. There were three biological replicates of KO cells and WT cells. Principal-component analysis (PCA) showed distinct differences in proteins between the KO and WT groups (Figure 3A). According to our data, there were 1,184 differentially expressed proteins (DEPs) among 10,074 detectable proteins ($|\log_2 FC| > 1$ and $p < 0.05$), with 542 upregulated and 642 downregulated proteins (Figures 3B and 3C). As shown in Figures S2A and S2B, the isoelectric point distribution map and sample expression distribution map indicated that the data quality control was reliable.

Gene Ontology (GO) enrichment analysis revealed that the enriched clusters were related to small-molecule metabolic process, lipid metabolic process, and steroid metabolic process in biological processes, and oxidoreductase activity, acid-thiol ligase activity, and monooxygenase activity in molecular functions, as shown in Figure 3D. The top 3 upregulated processes were cytoskeleton organization, regulation of cellular process, and muscle structure development in biological processes; non-membrane-bounded organelle, intracellular non-membrane-bounded organelle, and chromosome in cellular component; and DNA binding, transcription regulator activity, and cytoskeletal protein binding in molecular functions (Figure S2C). The top 3 downregulated processes were small-molecule metabolic process, lipid metabolic process, and organic acid metabolic process in biological processes; intrinsic component of membrane, integral component of membrane, and mitochondrial matrix in cellular component; and oxidoreductase activity, catalytic activity, and oxidoreductase activity acting on the CH-OH group of donors in molecular functions (Figure S2D). KEGG enrichment analysis revealed that the enriched clusters were related to peroxisome and ferroptosis in cellular processes, and fatty acid metabolism, fatty acid degradation, and fatty acid biosynthesis in metabolism, as shown in Figure 3E. The top 5 upregulated pathways were homologous recombination, cytoskeleton in muscle cells, signaling pathways regulating pluripotency of stem cells, lysine degradation, and proteoglycans in cancer (Figure S2E). The top 5 downregulated pathways were metabolic pathways, peroxisome proliferators-activated receptor (PPAR) signaling pathway, carbon metabolism, steroid biosynthesis, and fatty acid degradation (Figure S2F).

OSBPL2 deficiency alters the sensitivity of hepatocytes to ferroptosis

A recent study has reported that abnormal iron accumulation exists in the liver of patients with MASLD and that inhibiting ferroptosis can alleviate fibrosis.[11] Our proteomics data revealed that a series of metabolic processes and signaling pathways were altered in the KO cells, including ferroptosis. Based on this, we sought to investigate the role of OSBPL2 in iron metabolism in hepatocytes. We exposed HepG2 cells to the ferroptosis inducer RSL3 and observed a lower proportion of small LDs (diameter <5 μm) and a higher proportion of large LDs (diameter >5 μm) in the RSL3 group compared to that in the control group, which was similar to the OA group. This indicated that triggering ferroptosis could enlarge LDs (Figure 3F). Comparable observations were also made in Huh7 cells (Figure S3A). Moreover, immunofluorescence staining demonstrated that OSBPL2 was distributed on and around the LD surface in HepG2 and Huh7 cells after treatment with OA or RSL3 (Figures 3F and S3A). These findings suggested that OSBPL2 might also regulate the distribution of fatty acids and the lipolysis process of LDs in ferroptotic cells.

We next assessed the sensitivity of KO cells to ferroptosis. The KO cells and WT cells were treated with or without RSL3 and then labeled for Fe (II) using a fluorescent probe. Our findings revealed that KO cells exhibited lower fluorescence intensity of Fe (II) compared to WT cells after RSL3 exposure (Figures 3G and 3H), suggesting that OSBPL2 deficiency suppresses intracellular Fe (II) accumulation. Next, we labeled the oxidized and reduced states of lipids with a fluorescent probe (BODIPY C11) to evaluate lipid peroxide levels following RSL3 treatment. The results indicated a lower oxidized state/reduced state ratio in KO cells compared to WT cells (Figures 3I and 3J), implying that OSBPL2 deficiency mitigates the lipid peroxidation induced by RSL3. We assessed cell viability at various RSL3 concentrations using the CCK-8 assay and found that the KO cells demonstrated higher viability than WT cells (Figure 3K). To further confirm this finding, we performed small interfering RNA (siRNA) interference in Huh7 cells. The qPCR results showed that siRNA #2 most effectively downregulated OSBPL2 expression (Figure S3B). Western blot analysis confirmed the absence of the OSBPL2 band in cells transfected with siRNA #2 (Figure S3C). The cell viability results of Huh7 cells transfected with siRNA #2 were similar to those observed in KO cells, with higher viability in OSBPL2-knockdown cells within the RSL3 concentration range of 12.5–25 μM (Figure S3D). Western blot analysis showed that glutathione peroxidase 4 (GPX4) expression was decreased in RSL3-treated WT cells, whereas OSBPL2-knockdown cells were not affected. In addition, inhibition of OSBPL2 expression significantly suppressed the expression of nuclear receptor coactivator 4 (NCOA4), a key gene involved in ferritinophagy (Figure S3E).

Taken together, the above results indicated that OSBPL2 deficiency confers ferroptosis resistance.

(B) HepG2 cell lines were treated with oleic acid (OA) or cholesterol (CHOL) for 24 h. Then they were fixed and stained with BODIPY 493/503 to identify LD. Scale bars, 10 μm.
(C) Targeted metabolomics analysis revealed fatty acids profiles of WT and KO HepG2 cell lines ($n = 6$) via OPLS-DA.
(D) Fatty acids data of WT and KO HepG2 cell lines was used to identify differential metabolites by heatmap.
(E) Differential fatty acids in WT and KO HepG2 cell lines enriched in pathway were shown in KEGG analysis.
(F) Fluorescence images of LDs in the WT cells and KO cells stained with BODIPY 493/503 (green) during lipolysis. Scale bar, 100 μm.
(G) The dynamic changes of LDs on lipolysis in the HepG2 cells related to (F).
(H) Fluorescence images of LDs in the WT cells and KO cells stained with BODIPY 493/503 (green) during lipogenesis. Scale bar, 100 μm.
(I) qPCR was used to analyze the mRNA levels of FASN and SCD1 in the WT and KO HepG2 cell lines, ns: not significant.

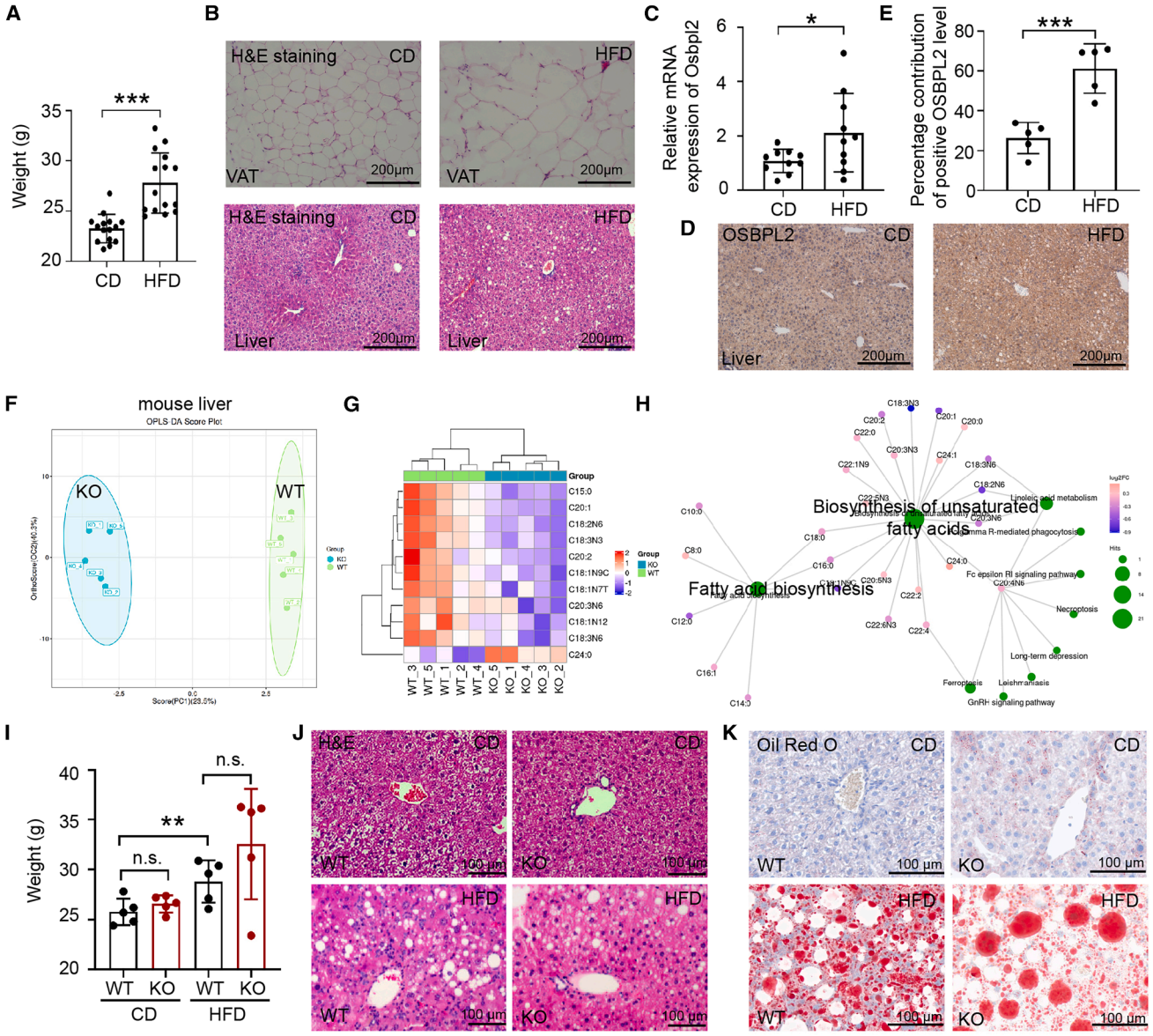

Figure 2. Liver fatty acids distribution and liver morphological characteristics in OSBPL2-deficient mice

(A) Body weight of mice fed with CD or HFD (CD group, n = 15; HFD group, n = 15).

(B) H&E-stained histological sections indicating the morphology of the visceral adipose tissue (VAT) and liver tissue. Scale bar, 200 μm.

(C) qPCR was used to analyze the mRNA levels of Osbpl2 in liver tissues of mice fed with CD or HFD (CD group, n = 10; HFD group, n = 10).

(D) Tissue sections in liver tissues were immune-stained with anti-OSBPL2 antibody using IHC. Scale bar, 200 μm.

(E) Percentage contribution of positive of OSBPL2 indicating OSBPL2 expression (CD group, n = 5; HFD group, n = 5) related to (D).

(F) Targeted metabolomics analysis revealed fatty acids profiles of WT and KO liver tissues (n = 5) via OPLS-DA.

(G) Fatty acids data of WT and KO liver tissues were used to identify differential metabolites by heatmap.

(H) Differential fatty acids in WT and KO liver tissues enriched in pathway were shown in KEGG analysis.

(I) Body weight of WT and KO mice fed with CD or HFD (n = 5).

(J) H&E-stained histological sections indicating the morphology of the liver tissue. Scale bars, 100 μm.

(K) Oil Red O-stained histological sections indicating the morphology of the liver LDs. Scale bars, 100 μm; The data are presented as the mean ± SD values ($n \geq 3$).

*$p < 0.05$; **$p < 0.01$, ***$p < 0.001$, ns, not significant.

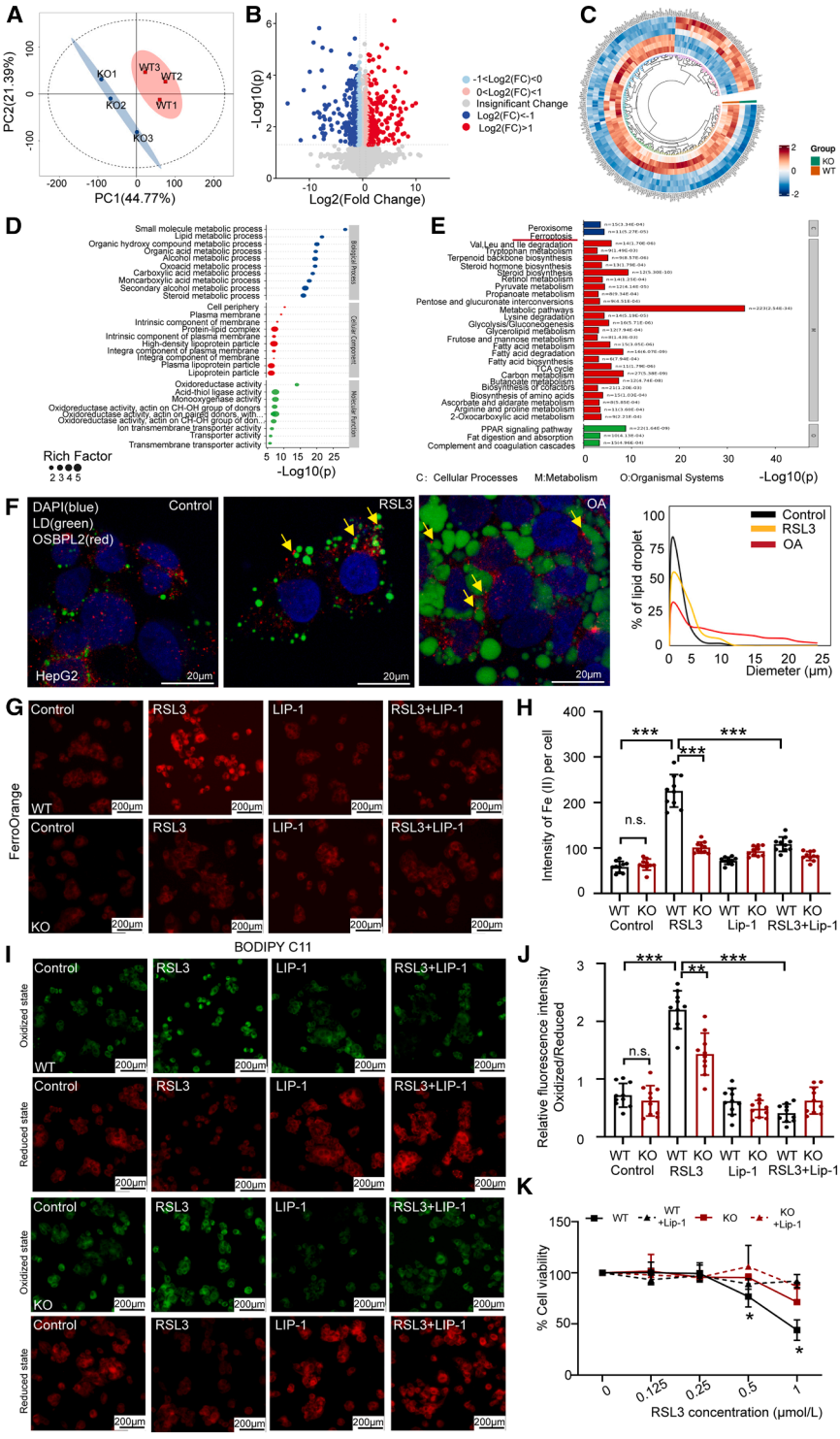

Figure 3. OSBPL2 deficiency reduces cell sensitivity of HepG2 cell lines to ferroptosis

(A) Proteomics analysis revealed proteins profiles of WT and KO HepG2 cell lines (n = 3) via PCA.

(B) Proteins data were used to identify differential proteins by volcano plot. Red and blue dots respectively indicated the upregulated and downregulated proteins.

(C) Proteins data were used to identify differential proteins by circle-heatmap.

(D–E) Differential proteins enriched in pathway were shown in GO and KEGG analysis.

(F) HepG2 cell lines were treated with RSL3 or OA for 24 h. Then they were fixed and immune-stained with anti-OSBPL2 (red). The nucleus was stained with DAPI (blue) and the LD was stained with BODIPY 493/503. Scale bars, 20 μm.

(G–H) The WT and KO HepG2 cell lines were treated with 500 nM RSL3 or 200 nM liproxstatin-1 (Lip-1) for 24 h. Then they were fixed and stained with FerroOrange (red) to identify Fe (II). Scale bars, 200 μm.

(I–J) The WT and KO HepG2 cell lines were stained with BDP 581/591 C11 to identify oxidized state of lipid peroxide (green) and reduced state of lipid peroxide (red). Scale bars, 200 μm.

(K) The WT and KO HepG2 cell lines treated with or without Lip-1, then they were treated with RSL3 at indicated concentration for 24 h. The cell viability was detected with a CCK8 biochemical detection assay (n = 3). The data are presented as the mean ± SD values ($n \geq 3$). $^{*}p < 0.05$; $^{**}p < 0.01$, $^{***}p < 0.001$, ns, not significant.

ACSL4 is downregulated in KO cells

To explore the underlying regulatory mechanism of OSBPL2 deficiency in ferroptosis, we combined the DEPs related to the ferroptosis pathway and those related to the fatty acid metabolism pathway in the proteomics data. As shown in Figures 4A and 4B, the heatmap and Venn diagram revealed that there are 4 DEPs that both existed in the ferroptosis pathway and the fatty acid metabolism. They are ACSL4, ACSL1, ACSL5, and ACSL6 (Figure 4C). Based on the literature review, ACSL4 stands out as the crucial rate-limiting enzyme that catalyzes PUFAs, specifically arachidonic acid (AA) and adrenic acid (AdA), followed by the induction of ferroptosis. In contrast, ACSL1 plays a pivotal role in mediating ferroptosis induced by α-eleostearic acid (αESA). To determine which of these four genes plays a greater role in MAFLD, we retrieved the expressions of these four genes using SteatoSITE (https://steatosite.com/), a metabolic dysfunction-associated steatohepatitis (MASH) RNA sequencing (RNA-seq) database derived from a retrospective multicenter national cohort of 940 MAFLD patients. In SteatoSITE, patients were stratified into five groups (control, F0/1, F2, F3, and F4) according to the MASH-Clinical Research Network (CRN) score. We found that as the MASH score increased, the expression of ACSL4

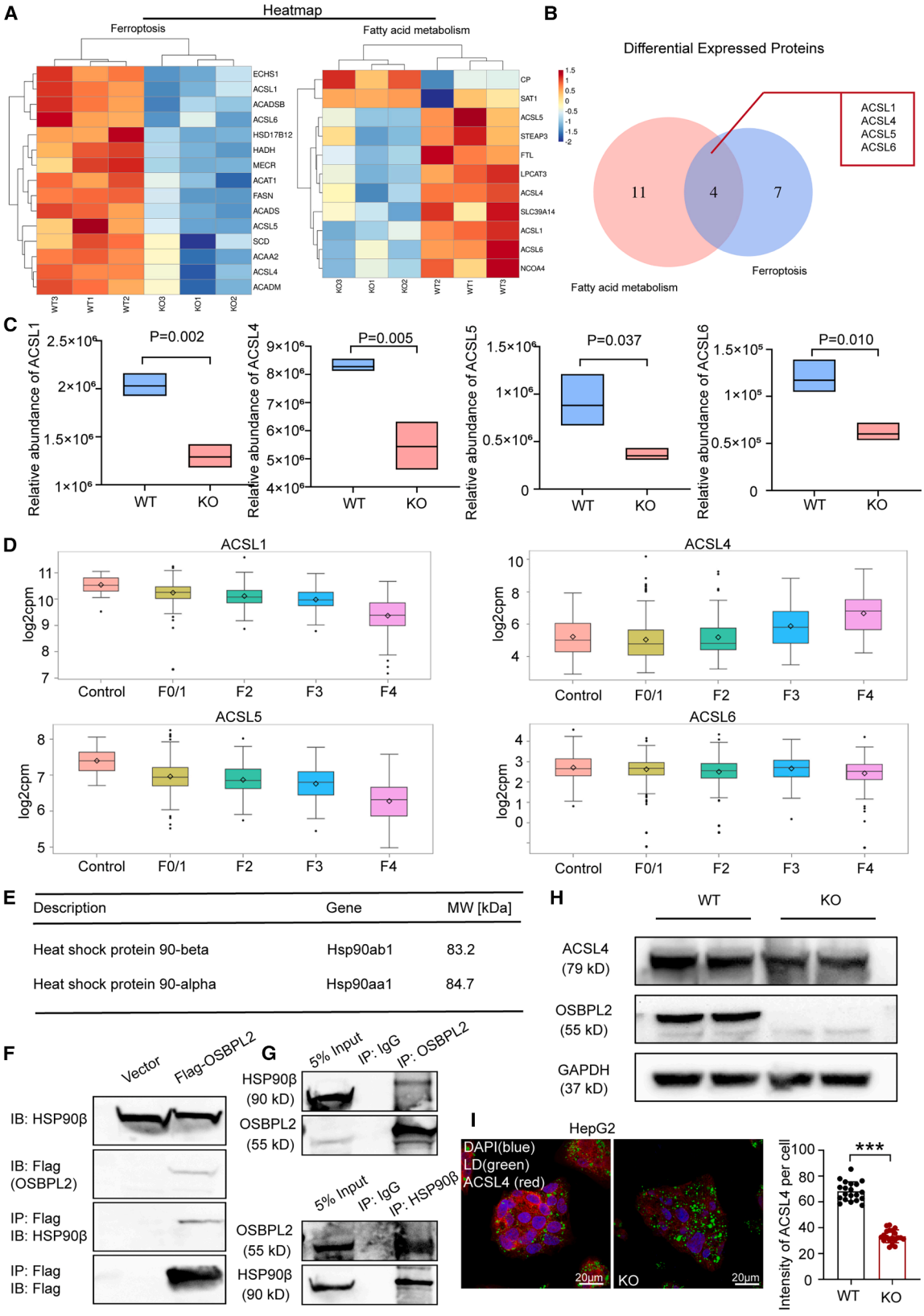

(legend on next page)

escalated, while the expressions of long-chain fatty acid–CoA ligase 1 (ACSL1) and long-chain fatty acid–CoA ligase 5 (ACSL5) diminished, and the expression of long-chain fatty acid–CoA ligase 6 (ACSL6) remained unaltered (Figure 4D). In addition, in our proteomics data, ACSL4 exhibited the highest abundance among the four candidate proteins. Furthermore, α-ESA was not detected in our fatty acid metabolomics data, so we thus selected ACSL4 as the primary target for our study.

In our previous studies, we identified a large number of OSBPL2-interacting proteins through proteomic analysis.[6] Based on published literature, we screened out heat shock protein (HSP90)-alpha (HSP90α) and HSP90-beta (HSP90β) (Figure 4E). It has been reported that HSP90 regulates ferroptosis in glioblastoma via ACSL4,[12] and we hypothesized that OSBPL2 may regulate ACSL4 expression through protein-protein interactions with these candidate proteins. The coimmunoprecipitation (CoIP) results showed that OSBPL2 bound to HSP90β (Figures 4F and 4G). We next performed western blot analyses in KO cells and found that ACSL4 was notably diminished in KO cells compared to their WT counterparts (Figure 4H). Following this, we employed immunofluorescence staining to visualize the expression and distribution of ACSL4 within the cells. Our observations indicated that KO cells contained a markedly higher number of LDs than WT cells (Figure 4I). Concurrently, the fluorescence intensity of ACSL4 in KO cells was significantly reduced compared to that in WT cells (Figure 4I). To corroborate our findings, we transfected Huh7 cells with siRNA and conducted qPCR and Western Blot (WB) analyses. Similar results were obtained from these experiments: inhibiting OSBPL2 expression downregulated ACSL4-RNA and protein expression levels, which further validated our initial observations (Figures S3F and S3G). Our results suggested that OSBPL2 binds to HSP90β, and that OSBPL2 deficiency inhibits ACSL4 expression.

LD changes the sensitivity of hepatocytes to ferroptosis

To further clarify the relationship between OSBPL2 and ferroptosis, we also investigated whether the fatty acid alterations caused by OSBPL2 deficiency could affect ACSL4 expression and thereby influence ferroptosis. According to our targeted metabolomic results, OA (C18:1N9C) and palmitic acid (16:0)—the two main fatty acids for triglyceride synthesis—were both decreased in KO cells, and the targeted metabolomic results of liver tissue exhibited a similar trend (Figure 5A), indicating that more LDs existed in KO cells and fewer fatty acids were released from LDs. Subsequently, we induced ferroptosis using RSL3 and found that the expression of FASN was significantly increased in KO cells after induction, whereas the expression of SCD1 was significantly elevated in WT cells (Figure 5B). The FASN-SCD1 pathway is the core route for *de novo* fatty acid synthesis and subsequent assembly into TAGs within cells. These results suggested that ferroptosis promoted *de novo* fatty acid synthesis. When LDs were induced prior to RSL3 treatment, the difference in cell viability between WT and KO cells was partially eliminated (Figures 3K and 5C). Because LDs are primarily composed of triglycerides and cholesterol esters, we induced LDs with OA or cholesterol, then labeled Fe (II) with a fluorescent probe (FerroOrange) to assess the fluorescence intensity of Fe (II). Our findings revealed that regardless of whether LDs were derived from TAGs or cholesterol, the average amount of Fe (II) was decreased (Figure 5D). To further validate these findings, we conducted similar experiments using a different cell line (Huh7) and obtained comparable results (Figure S3H). We then induced LDs and performed immunofluorescence staining to verify the expression of ACSL4. Our findings indicated that OA treatment led to a decrease in ACSL4 expression in both WT and KO cells compared to basal culture conditions, although the fluorescence intensity of ACSL4 remained lower in KO cells than in the WT group (Figures 4I and 5E). Additionally, under OA induction, we observed a significant increase in the number of nuclear LDs (nLDs) specifically in KO cells compared to the WT group.

These results indicated the existence of LDs could alter the sensitivity of hepatocytes to ferroptosis, further suggesting that the inhibition of LD lipolysis caused by OSBPL2 deficiency might confer ferroptosis resistance.

The lack of OSBPL2 inhibits the ACSL4/PUFA pathway

Given that PUFAs are substrates of ACSL4, we checked the concentrations of (AA, C20:4N6), (AdA, C22:4), and the precursor fatty acids of AA—such as linoleic acid (C18:2N6) and γ-linolenic acid (C18:3N6)—from the targeted metabolomic data of HepG2 cells and liver tissues. We found that only linoleic acid was decreased in both KO cells and KO tissues; γ-linolenic acid was decreased in KO tissues but not in KO cells (Figure 5F). These results suggested that OSBPL2 deficiency might affect AA generation. However, according to the targeted metabolomic data, neither AA nor AdA was decreased in either KO cells or KO

Figure 4. OSBPL2 deficiency reduces the expression of ACSL4

(A) Proteomics analysis revealed differential proteins in ferroptosis and fatty acid metabolism pathway by heatmap.

(B) Venn-diagram was used to show the differential proteins both in the two pathways.

(C) Differential protein abundance analysis was used to show relative abundance of candidate proteins.

(D) ACSL1, ACSL4, ACSL5, and ACSL6 were search in SteatoSITE (https://steatosite.com/), a NASH RNA-seq database from a retrospective multicentre national cohort of 940 NAFLD patients. In SteatoSITE, according to NASH-CRN score, patients were separated into five groups (control; F0/1, F2, F3, and F4).

(E) Proteomics analysis of the OSBPL2 interactome was used to show candidate proteins.

(F) HEK293T cells were transfected with FLAG-tagged OSBPL2 plasmid for 48 h. CoIP assays were used to verify the interaction of FLAG-tagged OSBPL2 with endogenous HSP90β.

(G) CoIP assays were used to verify the interaction of endogenous OSBPL2 with endogenous HSP90β in HepG2 cells.

(H) Lysates of the WT and KO HepG2 cell lines were immunoblotted for ACSL4, OSBPL2, and GAPDH. The data are normalized to the GAPDH control.

(I) HepG2 cell lines were fixed and immune-stained with anti-ACSL4 (red). The nucleus was stained with DAPI (blue) and the LD was stained with BODIPY 493/503. Scale bars, 20 μm (inserts, 10 μm). The data are presented as the mean ± SD values ($n \geq 3$). *$p < 0.05$; **$p < 0.01$, ***$p < 0.001$, ns, not significant.

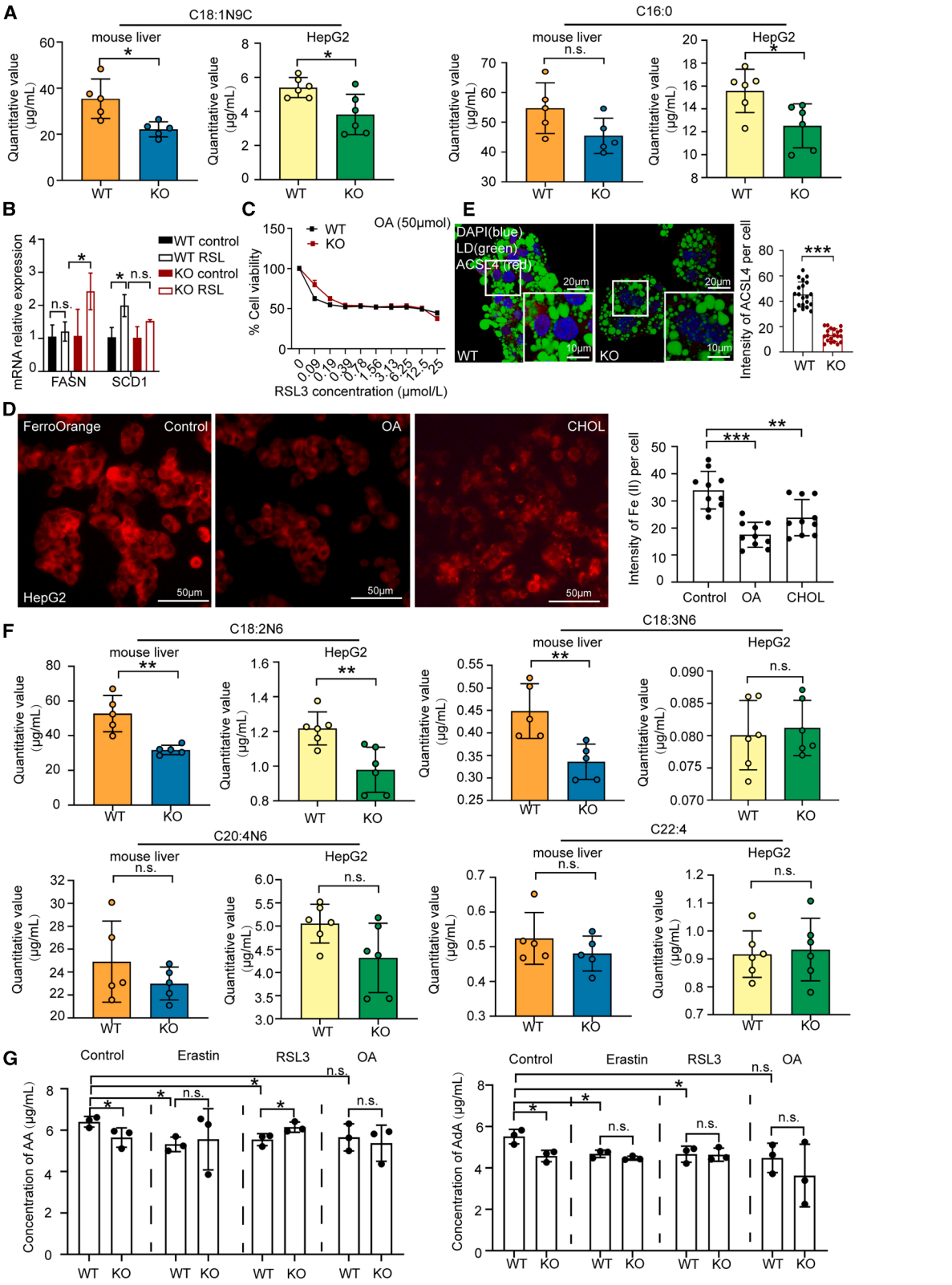

(legend on next page)

tissues (Figure 5F). These results suggested that the catalysis of AA or AdA was hindered, which might be caused by the downregulation of ACSL4. To further confirm this finding, we detected AA and AdA in HepG2 cells using ELISA. Our findings revealed significantly reduced AA and AdA levels in KO cells compared to WT cells under basal conditions (Figure 5G). Following this, we induced LDs or treated the cells with ferroptosis inducers (erastin and RSL3). Notably, erastin or RSL3 treatment led to a decrease in AA and AdA content in WT cells, indicating that free AA and AdA were catalytically utilized and ultimately converted into lipid peroxides. However, under RSL3 treatment, the content of AA in KO cells was higher than that in WT cells, indicating that OSBPL2 deficiency inhibited ACSL4's capacity to catalyze AA. When LDs were induced in WT cells, the levels of AA and AdA did not change, indicating that the addition of exogenous OA failed to alter AA and AdA levels under basal conditions (Figure 5G). These results implied that OSBPL2 deficiency could impede hepatocellular ferroptosis mediated by the ACSL4/PUFA pathway.

OSBPL2 deficiency alleviates HFD-induced hepatic fibrosis

To further verify the function of OSBPL2 in ferroptosis *in vivo*, OSBPL2-KO mice and their littermate WT mice were randomly allocated to be fed a CD or a HFD. We examined iron content in the livers of male mice. Under HFD feeding conditions, the KO group had significantly lower Fe (II) and total iron content in their livers compared to the WT group (Figures 6A and 6B). We collected serum and liver samples from the mice to assess PUFA content. We found a significant decrease in AA levels in both serum and liver tissue of mice subjected to HFD feeding (Figures 6C and 6D). Furthermore, our observations indicated that regardless of whether the mice were fed a CD or a HFD, KO mice exhibited higher AA content than WT mice under equivalent conditions (Figures 6C and 6D). We also measured serum and liver malondialdehyde (MDA) levels. While no significant differences were observed in serum MDA levels among the groups, liver MDA levels were significantly higher in the HFD-WT group compared to the CD-WT group. Notably, under HFD conditions, liver MDA levels were lower in the KO group compared to the WT group, although the difference was not statistically significant (Figure 6E). To validate the aforementioned findings, we collected livers from male mice and isolated tissue proteins. Western blot analysis revealed that under HFD conditions, the livers of KO mice demonstrated reduced ACSL4 expression compared to those of WT mice (Figure 6F). These findings were concordant with our cell-based experiments.

Subsequently, serum alanine aminotransferase (ALT) and aspartate aminotransferase (AST) levels were examined to evaluate liver function. Specifically, in male mice, ALT levels were significantly increased in the HFD group compared with those in the CD group, while AST levels remained unchanged (Figures 6G and 6H). Conversely, in female mice, AST levels were elevated in the HFD group compared with those in the CD group, but no alteration was observed in ALT levels (Figures S1B and S1C). These findings indicated that HFD feeding did indeed impact liver function in mice; however, it is noteworthy that there was no significant difference between WT and KO mice. We then detected liver ALT and AST levels in the four groups. The results showed that ALT and AST levels in male mice under HFD were significantly increased, but no significant differences were observed between WT and KO mice (Figures 6G and 6H, S1H and S1I). Finally, total cholesterol and triglyceride levels were measured. HFD feeding was found to elevate liver cholesterol and triglyceride content. Notably, triglyceride content was higher in male mice from the HFD-KO group compared to the HFD-WT group (Figures 6I and 6J, S1J and S1K). Then Sirius red staining was employed to assess liver fibrosis. Under high-fat feeding conditions, the livers of WT male mice exhibited widespread red fibrous staining, indicating a liver fibrosis phenotype. Interestingly, this red staining was not prominent in female mice. More importantly, the Osbpl2-KO mice showed reduced red staining in both genders, implying that *Osbpl2* deficiency might hinder liver fibrosis in male mice (Figures 6K and S1F). Sirius red staining was then employed to assess liver fibrosis. Under high-fat feeding conditions, the livers of WT male mice exhibited widespread red fibrous staining, indicating a liver fibrosis phenotype. Interestingly, this red staining was not prominent in female mice. More importantly, Osbpl2-KO mice showed reduced red staining in both genders, implying that Osbpl2 deficiency might alleviate liver fibrosis in male mice. To further investigate the effect of Osbpl2 deficiency on collagen fiber types, we conducted polarized light microscopy based on Sirius red staining. The results indicated that both WT and KO mice had yellow and green collagen fibers, corresponding to type I and III collagen fibers, with no significant difference between the two groups

Figure 5. Impact of ACSL4/PUFA pathway in OSBPL2-deficient HepG2 cell lines

(A) Targeted metabolomics analysis revealed the abundance of oleic acid (C18:1N9C) and palmitic acid (16:0).

(B) qPCR was used to analyze the mRNA levels of FASN and SCD1 in the WT and KO HepG2 cells treated with or without RSL3.

(C) The WT and KO HepG2 cell lines treated with OA to induce LDs, then they were treated with or without RSL3 at indicated concentration for 24 h. The cell viability was detected with a CCK8 biochemical detection assay ($n = 3$).

(D) HepG2 cell lines were treated with oleic acid (OA) or cholesterol (CHOL) for 24 h. Then they were fixed and stained with FerroOrange (red) to identify Fe (II). Scale bars, 50 μm.

(E) HepG2 cell lines were treated with OA for 24 h, then they were fixed and immune-stained with anti-ACSL4 (red). The nucleus was stained with DAPI (blue) and the LD was stained with BODIPY 493/503. Scale bars, 20 μm (inserts, 10 μm).

(F) Targeted metabolomics analysis revealed the abundance of linoleic acid (C18:2N6), γ-linolenic acid (C18:3N6), arachidonic acid (AA, C20:4N6), and adrenic acid (AdA, C22:4).

(G) Concentration of AA or AdA in the WT and KO HepG2 cell lines treated with erastin, RSL3 or OA was detected with an ELISA assay kit ($n = 3$). The data are presented as the mean ± SD values ($n \geq 3$). $^{*}p < 0.05$; $^{**}p < 0.01$, $^{***}p < 0.001$, ns, not significant.

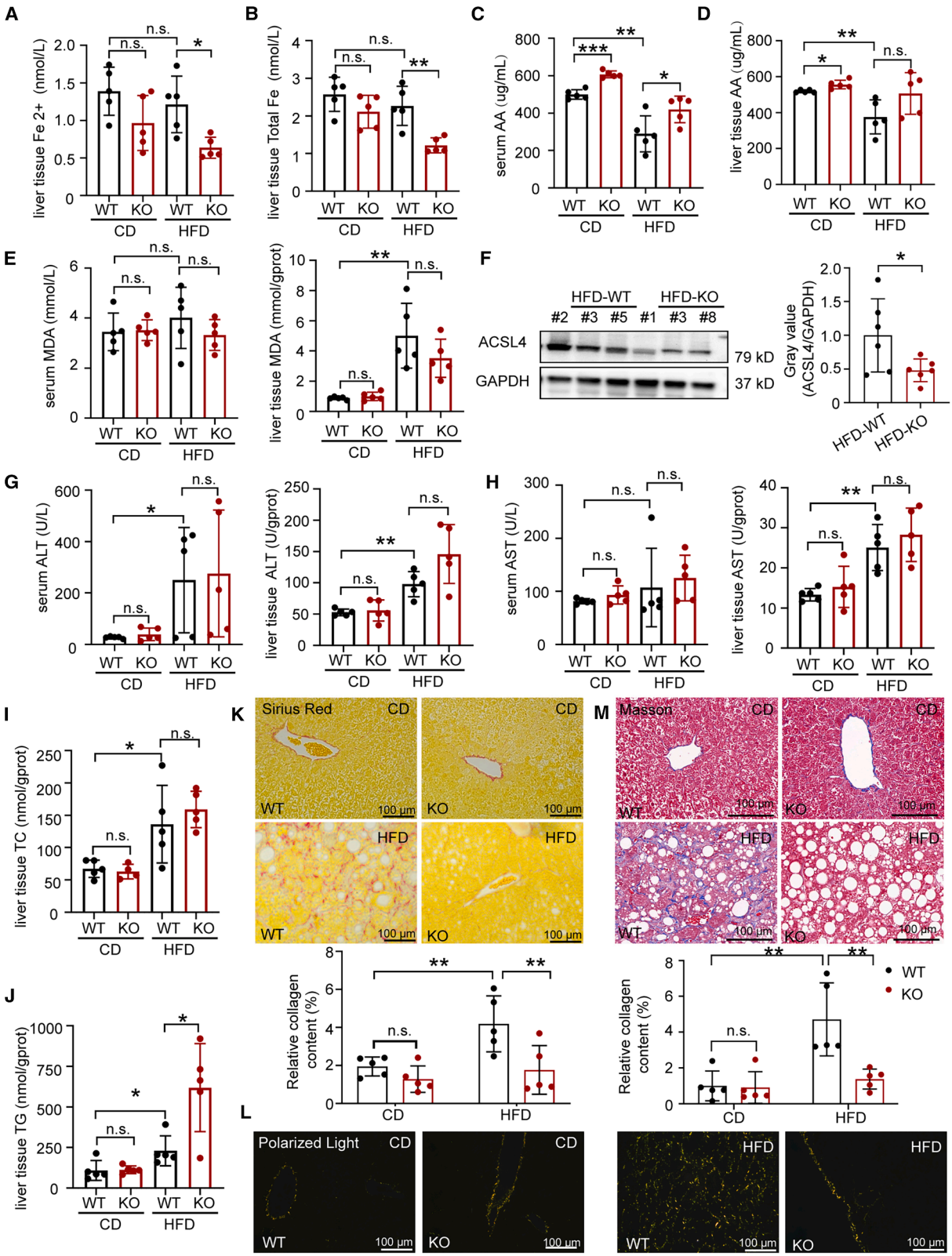

(legend on next page)

(Figure 6L). Subsequently, Masson staining was performed on the liver tissues, and the results were consistent with those of Sirius red staining (Figures 6M and S1G). The above results suggest that OSBPL2 deficiency inhibits liver fibrosis in male mice.

In conclusion, our findings suggest that OSBPL2 deficiency impairs LD lipolysis and alters fatty acid distribution in hepatocytes, which subsequently inhibits liver fibrosis by suppressing ferroptosis mediated by the ACSL4/PUFA pathway.

DISCUSSION

MASLD often arises from hepatic lipid accumulation caused by *de novo* lipogenesis or excess fatty acid transport to the liver.[13] Either increased lipolysis or excess dietary fatty acid intake can result in surplus fatty acids.[13] Therefore, unhealthy lifestyles and dietary patterns are important contributing factors to MAFLD. Minimizing sedentary behavior, engaging in regular physical activity, and making dietary modifications are recommended.[14] Fatty acid metabolism causes reactive oxygen species (ROS) generation and cellular oxidative damage, is one of the most important factors that drive MASLD development.[15] Consequently, reducing intracellular fatty acids can potentially mitigate the oxidative harm and slow down the development of MASLD. In this study, we reported that OSBPL2 deficiency altered the distribution of fatty acids in hepatocytes and alleviated liver fibrosis in male mice.

OSBPL2 deficiency alters the distribution of intracellular fatty acids. OSBPL2 is a member of the OSBP and OSBP-related protein family, which share a conserved ORD (OSBP-related protein domain) that primarily binds cholesterol. Besides cholesterol transport, some OSBP/ORPs, such as OSBPL2, OSBPL5, and OSBPL8, can affect the formation and breakdown of LDs.[16,17] It is reported that OSBPL5s locate at the ER-LD contacts, α-helices (AH domain) within the ORD of OSBPL5 is crucial for LD targeting, and the lack of OSBPL5 can cause LD enlargement.[18] Similarly, our previous research highlighted the role of OSBPL2 in LD metabolism, suggesting that OSBPL2 deficiency disrupts ER-LD contacts, impeding lipase's ability to target LDs.[9] In this study, we reported the lack of OSBPL2 caused intracellular LD accumulation and affected LD breakdown. In this study, we have added the detection of the expression of FASN and SCD1—the key enzymes involved in *de novo* fatty acid synthesis. We found that there's no difference in *de novo* fatty acid synthesis under basic condition in the WT and KO cells, but FASN expression was significantly increased when the cells treated with RSL3 in the KO cells. RSL3 treatment enhanced the *de novo* fatty acid synthesis pathway and increased the number of intracellular LDs, indicating that the total triglyceride content was elevated following RSL3 exposure. In contrast, our ELISA data showed that the AA level in KO cells was higher than that in WT cells after RSL3 treatment. This observation only indicates that the low expression of ACSL4 impairs its catalytic efficiency toward AA. However, we have not obtained evidence to confirm that these PUFAs can in turn promote triglyceride synthesis. In our previous studies, we reported that OSBPL2-KO restricted the translocation of patatin-like phospholipase domaincontaining 2 (PNPLA, also known as ATGL) from the endoplasmic reticulum to LDs, thereby inhibiting LD catabolism without affecting ATGL expression. Consequently, we did not investigate the impact of lipases on triglycerides, diglycerides, and monoglycerides. Liver LDs serve dual roles: they store excess FFAs to shield cells from lipid toxicity of fatty acids and they also release fatty acids to generate ATPs.[19] With the metabolomics analysis, our findings revealed notable changes in fatty acid distribution in the liver tissues of *Osbpl2*-KO mice and *OSBPL2*-KO cell lines. Specifically, oleic acid and palmitic acid, which are primary fatty acid components, were significantly reduced. This reduction may be attributed to the inhibition of LD breakdown. Given that ACSL4-catalyzed PUFA-mediated ferroptosis plays a crucial role in hepatic oxidative injury. Interestingly, we found that RSL3 treatment enhanced *de novo* fatty acid synthesis, which contributed to increased triglyceride accumulation. Notably, we observed significantly reduced liver fibrosis in *Osbpl2*-deficient mice, potentially linked to the inhibited decomposition of LDs and the subsequent easing of cell damage induced by fatty acid oxidation.

We discovered that a lack of OSBPL2 diminishes the hepatocellular sensitivity to ferroptosis. Ferroptosis plays a pivotal role in driving the progression of MASLD.[20] In a mouse model of MASH, a high-iron diet appeared to exacerbate the condition.[11] Iron plays a very important role in cellular energy metabolism. However, excess iron can impair mitochondrial function, increase the synthesis of saturated fatty acids, and promote the development and progression of MAFLD. These adverse effects are centered on the alteration of intracellular redox balance.[21,22] In our data of high-fat induced fatty liver mouse model, we found that male mice developed liver fibrosis, whereas female mice only exhibited steatosis without significant fibrosis. The potential significance of this gender difference may stem from differences in androgen levels. Androgens have been reported to promote

Figure 6. OSBPL2 deficiency alleviates HFD-induced liver fibrosis in male mice

(A-B) Concentration of Fe-(II) and total Fe in liver tissues of WT and KO mice fed with CD or HFD was detected with an iron assay kit ($n = 5$).

(C–D) Concentration of AA in in serum and liver tissues was detected with an ELISA assay kit ($n = 5$).

(E) Concentration of MDA in serum and liver tissues was detected with MDA biochemical assay kit ($n = 5$).

(F) Lysates of liver tissues were immunoblotted for ACSL4 and GAPDH. The data are normalized to the GAPDH control.

(G–H) Concentration of ALT and AST in serum and liver tissues from the WT and KO mice fed with CD or HFD ($n = 5$).

(I) Concentration of total cholesterol (TC) in liver tissues ($n = 5$).

(J) Concentration of triglyceride (TG) in liver tissues ($n = 5$).

(K–L) Sirius red-stained histological sections indicating the morphology of the liver fibrosis. Polarized light was used to indicate collagenous fibers. Scale bars, 100 μm.

(M) Masson-stained histological sections indicating the morphology of the liver fibrosis. Scale bars, 100 μm. The data are presented as the mean ± SD values ($n \geq 3$). *$p < 0.05$; **$p < 0.01$, ns, not significant.

ferroptosis in multiple organs.[23,24] A growing body of evidence supports the notion that males are more susceptible to ferroptosis-induced injury and subsequent development of hepatic fibrosis. Study on a cohort of 494 Asian patients with MASLD, has revealed higher iron content in the livers of male patients than that in the female ones.[11] Consequently, a therapeutic approach that targets ferroptosis to inhibit MASLD may prove more beneficial for male patients. The distribution of intracellular fatty acids can affect ferroptosis and the ACSL4-mediated ferroptosis pathway is critical for the development of hepatic fibrosis. PUFAs are prone to enzymatic and non-enzymatic oxidation, forming lipid hydroperoxides (L-OOH). These compounds are highly toxic to cells and cell membranes, triggering ferroptosis, which represents the primary pathway of this cell death mechanism. Unsaturated linoleic acid was employed to trigger ferroptosis by iron-dependent lipid peroxidation to treat high-grade serous ovarian cancer.[25] The AAs and AdAs generated from linoleic acid enhances the sensitivity of gastric cancer cells to ferroptosis.[26] Palmitic acid also make cancer cells become vulnerable to ferroptosis via endoplasmic reticulum stress.[27] Moreover, a fundamental study on liver cancer has revealed that boosting lipophagy within paclitaxel-tolerant persister cancer cells can augment the susceptibility of them to ferroptosis, ultimately attaining the goal of tumor elimination.[28] Our research further discovered Osbpl2-deficient liver tissues and cell lines exhibited significant decreases in the levels of linoleic acid and palmitic acid as well as oleic acid. Our *in vivo* and *in vitro* data showed that OSBPL2 deficiency led to LD accumulation and a decrease level of hepatocellular Fe (II), which further suggested that OSBPL2 deficiency diminishes hepatocellular sensitivity to ferroptosis. In addition, our results revealed ACSL4 was the key target. ACSL4 is a vital isozyme that catalyzes PUFAs including AA and AdA to form AA-CoA or AdA-CoA.[29,30] It is also an important therapeutic target for MASLD. Blockade of ACSL4-induced ferroptosis can ameliorate MASLD and MASH in mice.[11,31] However, there is still controversy over the role of ACSL4 in MASLD. A recent study has reported that liver parenchymal cell-specific deletion of ACSL4 fails to prevent disease progression in mouse models of MASLD.[32] Perhaps apart from liver parenchymal cells, other types of cells such as macrophages, T lymphocytes and B lymphocytes also play important roles. In our study, we performed proteomics to screen the major pathways and finally focus on ACSL4/PUFA-mediated ferroptosis pathway. Our results revealed that ACSL4 was downregulated in OSBPL2-deficient cells or liver tissues, which inhibited the ACSL4/PUFA-mediated ferroptosis.

MAFLD is increasingly prevalent in the adult population, and a worrying upward trend in diagnoses is observed in children and adolescents. In this context, an unhealthy diet—characterized by high energy intake, excessive fat intake, and unrefined carbohydrates—plays a significant role in the development and progression of the disease. Considering this situation, continuing to fortify foods with iron without updated population-level data on iron deficiency would be highly controversial rather than beneficial.[33] Under normal circumstances, iron-rich foods are beneficial to human health. However, in the MAFLD population, hepatic iron deposition is an inherent pathological feature. Consumption of iron-rich foods may further exacerbate the burden of hepatic iron metabolism, which in turn carries the risk of inducing hepatic ferroptosis and accelerating liver fibrosis. Whether it is necessary to formulate new, tailored dietary guidelines for populations with abnormal iron metabolism remains to be further investigated.

Generally speaking, OSBPL2 deficiency modifies the distribution of fatty acids in hepatocytes by impairing lipolysis, mitigates hepatocellular ferroptosis via the ACSL4/PUFA pathway, and delays the development of liver fibrosis. Our findings expand the role of OSBPL2 and provide valuable research data for the early intervention of MAFLD.

Limitations of the study

The data reported here address the regulation mechanism of OSBPL2 in ferroptosis and show that OSBPL2 deficiency can attenuate MASLD by conferring ferroptosis resistance. However, we acknowledge that the present study has several limitations, we did not employ transmission electron microscopy to better characterize the features of ferroptosis, apart from liver parenchymal cells, the role of other types of cells within liver tissues remains to be determined. In the future, our studies will focus on relationship of fatty acid, cholesterol, and hepatic microcirculation.

RESOURCE AVAILABILITY

Lead contact

Further information and requests for resources and reagents should be directed to and will be fulfilled by the lead contact, Jianquan Chen (jqchen@njmu.edu.cn).

Materials availability

This study did not generate new unique reagents.

Data and code availability

- The DIA proteomics data have been deposited to the ProteomeXchange Consortium (https://proteomecentral.proteomexchange.org) via the iProX partner repository. Accession numbers are listed in the key resources table.
- This paper does not report original code.
- Any additional information required to reanalyze the data reported in this paper is available from the lead contact upon request.

ACKNOWLEDGMENTS

This work was supported by the National Natural Science Foundation of China (grant no. 82200642) to T.W. and Talent Recruitment Fund of Nanjing Jiangning Hospital (grant no. 201701) to J.C.

AUTHOR CONTRIBUTIONS

T.W., writing – original draft, writing – review and editing, methodology, investigation, funding acquisition, and conceptualization; F.S., C.L., and Z.L., methodology and investigation; J.Y., formal analysis; X. Cao, conceptualization and formal analysis; X. Chen., writing – review and editing, and project administration; J.C., project administration, funding acquisition, and conceptualization.

DECLARATION OF INTERESTS

The authors declare no competing interests.

STAR★METHODS

Detailed methods are provided in the online version of this paper and include the following:

- KEY RESOURCES TABLE
- EXPERIMENTAL MODEL AND STUDY PARTICIPANT DETAILS
  - Cell lines
  - Animals
- METHOD DETAILS
  - Western blot analysis
  - Coimmunoprecipitation (CoIP)
  - Total RNA isolation and qRT-PCR analysis
  - Lipid droplet detection
  - Labile Fe (II) detection
  - Lipid peroxidation detection
  - Immunofluorescence
  - Tissue iron quantification
  - Arachidonic acid and adrenaline acid detection
  - Metabolomics analysis
  - DIA proteomics analysis
- QUANTIFICATION AND STATISTICAL ANALYSIS

SUPPLEMENTAL INFORMATION

Supplemental information can be found online at https://doi.org/10.1016/j.isci.2026.115478.

Received: September 8, 2025
Revised: January 30, 2026
Accepted: March 20, 2026
Published: March 25, 2026

REFERENCES

1. Israelsen, M., Francque, S., Tsochatzis, E.A., and Krag, A. (2024). Steatotic liver disease. Lancet Lond. Engl. *404*, 1761–1778.
2. Castera, L., Friedrich-Rust, M., and Loomba, R. (2019). Noninvasive Assessment of Liver Disease in Patients With Nonalcoholic Fatty Liver Disease. Gastroenterology *156*, 1264–1281.e4.
3. Walther, T.C., and Farese, R.V. (2012). Lipid droplets and cellular lipid metabolism. Annu. Rev. Biochem. *81*, 687–714.
4. Missaglia, S., Coleman, R.A., Mordente, A., and Tavian, D. (2019). Neutral Lipid Storage Diseases as Cellular Model to Study Lipid Droplet Function. Cells *8*, 187.
5. Takahashi, K., Kanerva, K., Vanharanta, L., Almeida-Souza, L., Lietha, D., Olkkonen, V.M., and Ikonen, E. (2021). ORP2 couples LDL-cholesterol transport to FAK activation by endosomal cholesterol/PI(4,5)P(2) exchange. EMBO J. *40*, e106871.
6. Wang, T., Zhang, T., Tang, Y., Wang, H., Wei, Q., Lu, Y., Yao, J., Qu, Y., and Cao, X. (2021). Oxysterol-binding protein-like 2 contributes to the developmental progression of preadipocytes by binding to β-catenin. Cell Death Discov. *7*, 109.
7. Yao, J., Zeng, H., Zhang, M., Wei, Q., Wang, Y., Yang, H., Lu, Y., Li, R., Xiong, Q., Zhang, L., et al. (2019). OSBPL2-disrupted pigs recapitulate dual features of human hearing loss and hypercholesterolaemia. J Genet Genomics *46*, 379–387.
8. Zhang, C., Zhang, H., Zhang, M., Lin, C., Wang, H., Yao, J., Wei, Q., Lu, Y., Chen, Z., Xing, G., and Cao, X. (2019). OSBPL2 deficiency upregulate SQLE expression increasing intracellular cholesterol and cholesteryl ester by AMPK/SP1 and SREBF2 signalling pathway. Exp. Cell Res. *383*, 111512.
9. Wang, T., Wei, Q., Liang, L., Tang, X., Yao, J., Lu, Y., Qu, Y., Chen, Z., Xing, G., and Cao, X. (2020). OSBPL2 Is Required for the Binding of COPB1 to ATGL and the Regulation of Lipid Droplet Lipolysis. iScience *23*, 101252.
10. Chen, X., Kang, R., Kroemer, G., and Tang, D. (2021). Broadening horizons: the role of ferroptosis in cancer. Nat. Rev. Clin. Oncol. *18*, 280–296.
11. Tao, L., Yang, X., Ge, C., Zhang, P., He, W., Xu, X., Li, X., Chen, W., Yu, Y., Zhang, H., et al. (2024). Integrative clinical and preclinical studies identify FerroTerminator1 as a potent therapeutic drug for MASH. Cell Metab. *36*, 2190–2206.e5.
12. Miao, Z., Tian, W., Ye, Y., Gu, W., Bao, Z., Xu, L., Sun, G., Li, C., Tu, Y., Chao, H., et al. (2022). Hsp90 induces Acsl4-dependent glioma ferroptosis via dephosphorylating Ser637 at Drp1. Cell Death Dis. *13*, 548.
13. Carli, F., Della Pepa, G., Sabatini, S., Vidal Puig, A., and Gastaldelli, A. (2024). Lipid metabolism in MASLD and MASH: From mechanism to the clinic. JHEP Rep. *6*, 101185.
14. Zeng, X.-F., Varady, K.A., Wang, X.D., Targher, G., Byrne, C.D., Tayyem, R., Latella, G., Bergheim, I., Valenzuela, R., George, J., et al. (2024). The role of dietary modification in the prevention and management of metabolic dysfunction-associated fatty liver disease: An international multidisciplinary expert consensus. Metabolism *161*, 156028.
15. Zhang, J., Ouyang, H., Gu, X., Dong, S., Lu, B., Huang, Z., Li, J., and Ji, L. (2024). Caffeic acid ameliorates metabolic dysfunction-associated steatotic liver disease via alleviating oxidative damage and lipid accumulation in hepatocytes through activating Nrf2 via targeting Keap1. Free Radic. Biol. Med. *224*, 352–365.
16. Guyard, V., Monteiro-Cardoso, V.F., Omrane, M., Sauvanet, C., Houcine, A., Boulogne, C., Ben Mbarek, K., Vitale, N., Faklaris, O., El Khallouki, N., et al. (2022). ORP5 and ORP8 orchestrate lipid droplet biogenesis and maintenance at ER-mitochondria contact sites. J. Cell Biol. *221*, e202112107.
17. Hynynen, R., Suchanek, M., Spandl, J., Bäck, N., Thiele, C., and Olkkonen, V.M. (2009). OSBP-related protein 2 is a sterol receptor on lipid droplets that regulates the metabolism of neutral lipids. J. Lipid Res. *50*, 1305–1315.
18. Du, X., Zhou, L., Aw, Y.C., Mak, H.Y., Xu, Y., Rae, J., Wang, W., Zadoorian, A., Hancock, S.E., Osborne, B., et al. (2020). ORP5 localizes to ER-lipid droplet contacts and regulates the level of PI(4)P on lipid droplets. J. Cell Biol. *219*, e201905162.
19. Mathiowetz, A.J., and Olzmann, J.A. (2024). Lipid droplets and cellular lipid flux. Nat. Cell Biol. *26*, 331–345.
20. Peleman, C., Hellemans, S., Veeckmans, G., Arras, W., Zheng, H., Koeken, I., Van San, E., Hassannia, B., Walravens, M., Kayirangwa, E., et al. (2024). Ferroptosis is a targetable detrimental factor in metabolic dysfunction-associated steatotic liver disease. Cell Death Differ. *31*, 1113–1126.
21. Barrera, C., Valenzuela, R., Rincón, M.Á., Espinosa, A., Echeverria, F., Romero, N., Gonzalez-Mañan, D., and Videla, L.A. (2018). Molecular mechanisms related to the hepatoprotective effects of antioxidant-rich extra virgin olive oil supplementation in rats subjected to short-term iron administration. Free Radic. Biol. Med. *126*, 313–321.
22. Valenzuela, R., Rincón-Cervera, M.Á., Echeverría, F., Barrera, C., Espinosa, A., Hernández-Rodas, M.C., Ortiz, M., Valenzuela, A., and Videla, L.A. (2018). Iron-induced pro-oxidant and pro-lipogenic responses in relation to impaired synthesis and accretion of long-chain polyunsaturated fatty acids in rat hepatic and extrahepatic tissues. Nutr. Burbank Los Angel. Cty. Calif *45*, 49–58.
23. An, K., Tan, Y., Yang, K., Kang, Y., Liu, P., Hao, B., Kang, J., and Su, J. (2025). Androgen-induced ferroptosis regulates seasonal testicular regression: insights into adaptive mechanisms of seasonal breeding. BMC Genom. *26*, 644.
24. Li, X., Lin, Y., Cheng, X., Yao, G., Yao, J., Hu, S., Zhu, Q., Wang, Y., Ding, Y., Lu, Y., et al. (2024). Ovarian ferroptosis induced by androgen is involved in pathogenesis of PCOS. Hum. Reprod. Open *2024*, hoae013.
25. Chen, Y., Liao, X., Jing, P., Hu, L., Yang, Z., Yao, Y., Liao, C., and Zhang, S. (2022). Linoleic Acid-Glucosamine Hybrid for Endogenous Iron-Activated

Ferroptosis Therapy in High-Grade Serous Ovarian Cancer. Mol. Pharm. *19*, 3187–3198.

26. Lee, J.-Y., Nam, M., Son, H.Y., Hyun, K., Jang, S.Y., Kim, J.W., Kim, M.W., Jung, Y., Jang, E., Yoon, S.J., et al. (2020). Polyunsaturated fatty acid biosynthesis pathway determines ferroptosis sensitivity in gastric cancer. Proc. Natl. Acad. Sci. USA *117*, 32433–32442.

27. Zhang, X., Liu, J., Bai, C., Fan, Y., Song, H., Huang, Z., Li, Y., and Luo, T. (2025). Palmitic acid enhances the sensitivity of ferroptosis via endoplasmic reticulum stress mediated the ATF4/TXNIP Axis in polycystic ovary syndrome. Phytomedicine *142*, 156777.

28. You, J.H., Lee, J., and Roh, J.-L. (2021). PGRMC1-dependent lipophagy promotes ferroptosis in paclitaxel-tolerant persister cancer cells. J. Exp. Clin. Cancer Res. *40*, 350.

29. Cui, J., Chen, Y., Yang, Q., Zhao, P., Yang, M., Wang, X., Mang, G., Yan, X., Wang, D., Tong, Z., et al. (2024). Protosappanin A Protects DOX-Induced Myocardial Injury and Cardiac Dysfunction by Targeting ACSL4/FTH1 Axis-Dependent Ferroptosis. Adv. Sci. *11*, e2310227.

30. Kagan, V.E., Mao, G., Qu, F., Angeli, J.P.F., Doll, S., Croix, C.S., Dar, H.H., Liu, B., Tyurin, V.A., Ritov, V.B., et al. (2017). Oxidized arachidonic and adrenic PEs navigate cells to ferroptosis. Nat. Chem. Biol. *13*, 81–90.

31. Duan, J., Wang, Z., Duan, R., Yang, C., Zhao, R., Feng, Q., Qin, Y., Jiang, J., Gu, S., Lv, K., et al. (2022). Therapeutic targeting of hepatic ACSL4 ameliorates NASH in mice. Hepatol. Baltim. Md *75*, 140–153.

32. Angendohr, C., Koppe, C., Herebian, D., Schneider, A.T., Keysberg, L., Singer, M.T., Gilljam, J., Dille, M.A., Bode, J.G., Doll, S., et al. (2025). The ferroptosis mediator ACSL4 fails to prevent disease progression in mouse models of MASLD. Hepatol. Commun. *9*, e0684.

33. Videla, L.A., and Valenzuela, R. (2022). Perspectives in liver redox imbalance: Toxicological and pharmacological aspects underlying iron overloading, nonalcoholic fatty liver disease, and thyroid hormone action. Biofactors *48*, 400–415.

34. Shi, H., Wang, H., Zhang, C., Lu, Y., Yao, J., Chen, Z., Xing, G., Wei, Q., and Cao, X. (2022). Mutations in OSBPL2 cause hearing loss associated with primary cilia defects via sonic hedgehog signaling. JCI Insight *7*, e149626.

STAR★METHODS

KEY RESOURCES TABLE

REAGENT or RESOURCE	SOURCE	IDENTIFIER
Antibodies		
Anti-GAPDH antibody	ABclonal	Cat# A19056; RRID:AB_2862549
Anti-NCOA4 antibody	ABclonal	Cat# A5695; RRID:AB_2766454
Anti-GPX4 antibody	ABclonal	Cat# A1933 RRID:AB_2763960
Anti-DDDDK-Tag antibody	ABclonal	Cat# AE005;RRID: AB_2770401
Anti-ACSL4 antibody	HUABIO	Cat# ET7111-43 RRID:AB_3071100
Anti-OSBPL2 antibody	Proteintech	Cat# 14751-1-AP; RRID:AB_2156092
Anti-Rabbit IgG, HRP-linked antibody	ABclonal	Cat# AS014 RRID:AB_2769854
Anti-Mouse IgG, HRP-linked antibody	ABclonal	Cat# AS003; RRID:AB_2769851
Anti-Rabbit IgG, Fluor 546, antibody	Invitrogen	Cat# A10040; RRID: AB_2534016
Chemicals, peptides, and recombinant proteins		
Oleic acid	Sigma	Cat# O1008
Cholesterol	Sigma	Cat# C4951
DAPI	Sigma	Cat# F6057
RSL3	Selleck	Cat# S8155
Erastin	Selleck	Cat# S7242
Liproxstatin-1	Selleck	Cat# S7699
BODIPY 493/503	Invitrogen	Cat# D3922
TRIzol Reagent	Invitrogen	Cat# 15596018
FerroOrange	DOJINDO	Cat# F374
BDP 581/591 C11	DOJINDO	Cat# L267
Anti-DYKDDDDK (Flag) Affinity Gel	HUABIO	Cat# HAK21024
Goat serum	Gibico	Cat# 16210064
Fetal bovine serum	Biochannel	Cat# 16210065
DMEM	Biochannel	Cat# BC-*M*-004
High-fat diet	Xietong	Cat# XT310
Critical commercial assays		
Iron Assay Kit	DOJINDO	Cat# I291
Human Arachidonic acid Elisa Assay Kit	RENJIEBIO	Cat# RJ12643
Mouse Arachidonic acid Elisa Assay Kit	RENJIEBIO	Cat# RJ17198
Human Adrenaline acid Elisa Assay Kit	RENJIEBIO	Cat# RJ24974
Mouse Adrenaline acid Elisa Assay Kit	RENJIEBIO	Cat# RJ29487
HiScript II RT-PCR Kit	Vazyme	Cat# P611-01
SYBR qPCR Master Mix	Vazyme	Cat# Q341-02
One-Step PAGE gel	Vazyme	Cat# E303-C1
Deposited data		
DIA Proteomics data	This paper	PXD075796 (https://proteomecentral.proteomexchange.org)
Immunoblots images	This paper	N/A
Experimental models: Cell lines		
HepG2	Hycyte	Cat# TCH-C196
Huh 7	Hycyte	Cat# TCH-C217
293T	Hycyte	Cat# TCH-C101

(*Continued on next page*)

Continued

REAGENT or RESOURCE	SOURCE	IDENTIFIER
Experimental models: Organisms/strains		
Mouse: C57BL/6J	Animal core facility of Nanjing medical university	N/A
Oligonucleotides		
OSBPL2 siRNA, see Table S1	tsingke	N/A
Primers for GAPDH, OSBPL2, ACSL4, FASN, and SCD1, see Table S2	tsingke	N/A
Software and algorithms		
GraphPad Prism 8	Graph Pad Software	N/A
Fiji-ImageJ	ImageJ Software	N/A

EXPERIMENTAL MODEL AND STUDY PARTICIPANT DETAILS

Cell lines

The HepG2, Huh7 and 293T cell line (Hycyte, China) was used in this study. Both cell lines were authenticated using short tandem repeat (STR) profiling, and were confirmed to be free of mycoplasma contamination. All the cells were cultured in DMEM supplemented with 10% FBS in a humidified atmosphere containing 5% CO_2 at 37°C.

Animals

Animal studies utilized *Osbpl2* knockout (KO) mice on a C57BL/6J background constructed previously in our lab.[34] The KO mice and their WT littermate controls were fed with control diet (CD) for 1 month after weaning. At 2 months, the KO and WT mice were fed with or without high-fat diet (HFD) and grouped as KO-CD, KO-HFD, WT-CD and WT-HFD, respectively. All animals were raised in an animal room under SPF conditions (temperature: 24.1 °C; humidity: 55–60%; photoperiod: 12 h light/12 h dark) in the animal core facility of Nanjing medical university. Animal management was performed strictly in accordance with the protocol approved by the Institutional Animal Care and Use Committee (IACUC) of the Nanjing medical university (Permit Number: No.2409068). All surgical procedures were performed under anesthesia to minimize animal suffering.

METHOD DETAILS

Western blot analysis

Cells or hepatic tissue were lysed with RIPA buffer added with protease inhibitor cocktail for protein sample preparation. One-Step PAGE gel was used to separate protein samples. The primary antibody working solutions were prepared with primary antibodies which were diluted using diluting solution at 1:1000 and the secondary antibody working solutions were prepared with secondary antibodies which were diluted at 1:5000. The bands were visualized by a chemiluminescence method.

Coimmunoprecipitation (CoIP)

293T cells were co-transfected with FLAG-tagged *OSBPL2* plasmid for 48 h. Then samples were washed 2–3 times with ice-cold PBS and lysed for 30 min with RIPA lysis buffer containing protease and phosphatase inhibitor cocktail. The lysate was centrifuged for 15 min at 12,000 rpm and 4°C. The supernatant was collected and incubated overnight with Anti-DYKDDDDK (Flag) Affinity Gel at 4°C. The lysate from the cells transfected with vector plasmid was extracted and immunoprecipitated as a negative control. The beads were washed more than five times, added to 6×SDS loading buffer and boiled for 5–10 min. Then, the samples were assayed by western blotting.

Total RNA isolation and qRT-PCR analysis

The TRIzol reagent was used for Total RNA isolation. The cDNA was obtained using a reverse transcription kit. The qRT-PCR was performed with a qPCR detection kit on an Applied Biosystems QuantStudio 5.

Lipid droplet detection

Cells were grown on coverslips (ø14mm) in 24-well plates overnight. BODIPY 493/503 was diluted in 10 mM PBS (pH 7.4) at 1:1000 to prepare working solution. Then samples were stained in a dark incubator at 37°C. After a 30 min incubation, the working solution was removed from 24-well plates. Fluorescent microscope was used to acquire high-quality images.

Labile Fe (II) detection

Cells were grown on coverslips (ø14mm) in 24-well plates overnight. Following the steps in the instruction manual, FerroOrange was diluted in PBS at 1:1000 to prepare working solution. Then samples were stained in a dark incubator at 37°C. After a 30 min incubation, samples were imaged immediately without the removement of working solution using a fluorescent microscope.

Lipid peroxidation detection

Cells were grown coverslips (ø14mm) in 24-well plates overnight. Following the steps in the instruction manual, the samples were stained in BDP 581/591 C11 working solution for 30 min at 37°C in a dark chamber. Then the cells were washed with HBSS twice to remove fluorescence probe. The images were acquired using fluorescent microscope.

Immunofluorescence

Cells were grown on coverslips (ø14mm) in 24-well plates overnight. The samples in 24-well plates were fixed, penetrated and then blocked with goat serum (used at 1:10 dilution). After that, the coverslips were incubated overnight with primary antibodies (used at 1:100 dilution) at 4°C and incubated with secondary antibodies for 1 h at 37°C. A antifade mounting medium containing DAPI was used to show nucleus. A laser scanning confocal microscope was used to acquire fluorescence images.

Tissue iron quantification

Following the steps in the instruction manual of Iron Assay Kit, after washing with ice-cold PBS, the tissues were grinded. The samples were divided into 3 parts: two parts were used for the detection of Fe (II) and total Fe, the rest was used as blank control. The reducer solution in Iron Assay Kit was added in the sample to detect total Fe. Samples were then incubated following the steps in the instruction manual. According to the absorbance (593 nm) detected using an automatic biochemical analyzer, draw the standard curve and calculate the tissue total iron content and Fe (II) levels.

Arachidonic acid and adrenaline acid detection

According to the instruction manual: for tissue detection, 1 g sample was grinded in 9 mL PBS (pH 7.2–7.4); for cell detection, Arachidonic acid (AA) or Adrenaline acid (AdA) was extracted from 10^6 cells by repeated freezing and thawing of liquid nitrogen. AA and AdA concentration were detected with Elisa Assay Kit. According to the absorbance (450 nm) detected using an automatic biochemical analyzer, draw the standard curve, calculate the AA and AdA levels.

Metabolomics analysis

Fresh liver samples were washed with ice-cold PBS twice, quick-freezed with liquid nitrogen and then kept at −80 °C. Metabolomics profiling was analyzed using a UPLC-ESI-Q-Orbitrap-MS systemcoupled with Q-Exactive Plus. Samples were analyzed using a ACQUITY UPLC HSS T3 column. Metabolomics were analyzed by Shanghai Bioprofile.

DIA proteomics analysis

The cell samples were washed with ice-cold PBS twice, then were collected from culture flask and quick-freezed with liquid nitrogen and then kept at −80 °C. LC-MS/MS were performed on a Orbitrap Astral mass spectrometer coupled with Vanquish *Neo* UHPLC system. DIA proteomics were analyzed by Shanghai Bioprofile.

QUANTIFICATION AND STATISTICAL ANALYSIS

Statistical analyses were performed in GraphPad Prism and all data were presented as the mean ± SD. Student's *t* test was used for comparisons between two independent sample groups, one-way analysis of variance (ANOVA) was used for single-factor comparisons among multiple groups, and two-way ANOVA was used for two-factor comparisons among multiple groups; $p < 0.05$ was regarded as significant.